Monthly Notices of the ROYAL ASTRONOMICAL SOCIETY
MNRAS **446,** 4291–4300 (2015) doi:10.1093/mnras/stu2281

The H I-dominated low-surface-brightness galaxy KKR 17

M. I. Lam,[1,2,3]★ H. Wu,[1,3] M. Yang,[1,3] Z.-M. Zhou,[1,3] W. Du[1,3] and Y.-N. Zhu[1,3]

[1] *National Astronomical Observatories, Chinese Academy of Sciences, Beijing 100012, China*
[2] *University of Chinese Academy of Sciences, Beijing 100049, China*
[3] *Key Laboratory of Optical Astronomy, National Astronomical Observatories, Chinese Academy of Sciences, 20A Datun Rd., Chao-Yang Dist., Beijing, 100012, China*

Accepted 2014 October 28. Received 2014 October 22; in original form 2014 August 11

ABSTRACT

We present new narrow-band (Hα and [O III]) images and optical spectrophotometry of H II regions for a gas-rich low-surface-brightness irregular galaxy, KKR 17. The central surface brightness of the galaxy is $\mu_0(B) = 24.15 \pm 0.03$ mag s^{-2}. The galaxy was detected by the Arecibo Legacy Fast ALFA survey (ALFALFA). Its mass is dominated by neutral hydrogen (H I) gas. In contrast, both the stellar masses of the bright H II and diffuse stellar regions are small. In addition, the fit to the spectral energy distribution to each region shows the stellar populations of H II and diffuse regions are different. The bright H II region contains a large fraction of O-type stars, revealing recent strong star formation, whereas the diffuse region is dominated by median age stars with a typical age of ∼600 Myr. Using McGaugh's abundance model, we found that the average metallicity of KKR 17 is 12 + (O/H) = 8.0 ± 0.1. The star-formation rate of KKR 17 is 0.21 ± 0.04 M$_\odot$ yr^{-1}, which is ∼1/5 of our Milky Way's. Based on the analysis results for young stellar clusters in the H II region, the bright H II region has two sub-components with different velocities and metallicities. This may be caused by the outflow of massive stars or merging events. However, the mechanism triggering star formation in the H II region is still uncertain.

Key words: galaxies: abundances – galaxies: evolution – galaxies: individual (KKR 17) – galaxies: irregular.

1 INTRODUCTION

Low-surface-brightness galaxies (LSBGs) are thought to be important baryonic contributors to the Universe (see Impey & Bothun 1997 and Bothun, Impey & McGaugh 1997 for reviews). The initial study by Freeman (1970), based on spiral galaxies, found that the central surface brightness of disk galaxies was concentrated in a very narrow range. Subsequently, Disney (1976) pointed out that the surface brightness results in Freeman (1970) may be due to a selection effect and predicted the existence of galaxies fainter than the sky background. Indeed, many surveys later discovered a large number of LSBGs (e.g. Schombert & Bothun 1988; Schombert et al. 1992; Bothun et al. 1992; Caldwell & Bothun 1987; Impey et al. 1996). They span a very wide range of morphologies (ranging from dwarfs and irregulars to giant disk galaxies), stellar masses and colours ($0.3 < B - V < 1.7$) (e.g. McGaugh, Schombert & Bothun 1995; O'Neil et al. 1997). Most LSBGs have low metallicity (see, e.g. Skillman, Kennicutt & Hodge 1989a; Skillman, Terlevich & Melnick 1989b), although the metallicities of some red LSBGs is around the solar metallicity (Bergmann, Jørgensen & Hill 2003).

Star formation plays a crucial role in the evolution of LSBGs. Usually, star formation in galaxies can be divided into four modes: (1) instantaneous star formation, typically in an interaction or merging event; (2) normal star formation with a relatively higher star-formation rate (SFR) (about 1–5 M$_\odot$ yr^{-1}), typically in normal spiral galaxies under gravitational wave density; (3) continuous star formation with a very low SFR over a long timescale, typically in dwarf galaxies (Schombert, Maciel & McGaugh 2011) and (4) episodic (sporadic) star formation, which is not a continuous process and has small fluctuations, typically in LSBGs (McGaugh 1994a). LSBGs have relatively low SFRs, probably an order of magnitude lower than high-surface-brightness galaxies (HSBGs) (Bothun et al. 1997; Kim 2007). Previous studies showed that the evolution of LSBGs was much slower than that of their high surface brightness counterparts (HSBGs), and most of their stellar mass was formed by the third star-formation mode. However, Schombert, McGaugh & Eder (2001) argued that the weak bursts and interaction may have occurred in LSBGs in the last 5 Gyr. Kim (2007) found that LSBGs may undergo episodic star formation in the Hubble time due to infalling gas. Recently, Schombert, McGaugh & Maciel (2013) and Schombert & McGaugh (2014) both found that the star-formation mechanism in their sample appeared to be the same as those of HSBGs, and the total stellar mass formation in LSBGs occurred

★ E-mail: linminyi@nao.cas.cn

© 2014 The Authors
Published by Oxford University Press on behalf of the Royal Astronomical Society

Downloaded from http://mnras.oxfordjournals.org/ at National Astronomical Observatory on March 8, 2015

Table 1. Observation log.

Band	Telescope	Instrument	λ_{eff} (μm)	Exposure time (s)	Date (UT)	FWHM (arcsec)	Pixel size (arcsec pixel^{-1})
FUV	*GALEX*	–	0.1516	1701.05	2009 May 28	6.0	1.500
NUV	*GALEX*	–	0.2267	1701.05	2009 May 28	6.0	1.500
u	SDSS	–	0.3543	53.9	2003 Jun 22	1.4	0.396
g	SDSS	–	0.4770	53.9	2003 Jun 22	1.4	0.396
r	SDSS	–	0.6231	53.9	2003 Jun 22	1.4	0.396
i	SDSS	–	0.7625	53.9	2003 Jun 22	1.4	0.396
z	SDSS	–	0.9134	53.9	2003 Jun 22	1.4	0.396
3.4 µm	*WISE*	–	3.368		2010	6.0	1.375
21 cm	Arecibo	*L*-band	21 cm	–	–	∼3.5 arcmin	–
			Our observations				
V	Xinglong 2.16 m	BFOCS	0.545	2 × 300	2012 Jun 16	2.2	0.45
R	Xinglong 2.16 m	BFOCS	0.700	2 × 300	2012 Jun 17	2.2	0.45
[O III]-4	Xinglong 2.16 m	BFOCS	0.516	2 × 1800	2012 Jun 16	2.2	0.45
Hα-5	Xinglong 2.16 m	BFOCS	0.676	3600	2012 Jun 17	2.2	0.45
Spectrum (G6)	Xinglong 2.16 m	BFOCS	0.33–0.545	3600	2013 Mar 10	3.0	0.45
Spectrum (G7)	Xinglong 2.16 m	BFOCS	0.39–0.67	3600	2013 Jun 15	1.8	0.45
Spectrum (G8)	Xinglong 2.16 m	BFOCS	0.58–0.82	3600	2012 Jun 17	2.2	0.45

in close to the Hubble time. Alternatively, the star-formation mode was normal. All of these results show that star-formation activities in LSBGs are still controversial.

To understand the evolution of LSBGs better, it is essential to study star formation in nearby LSBGs. Therefore, we selected one typical blue LSBG from Arecibo Legacy Fast ALFA Survey (ALFALFA) (Giovanelli et al. 2005), KKR 17, to investigate its possible star-formation activity. KKR 17 has one bright, compact knot, and one extended, faint diffuse region. This galaxy was first discovered by the Second Palomar Sky Survey (Karachentseva, Karachentsev & Richter 1999), and its red shift was confirmed to be 0.0276 (Makarov, Karachentsev & Burenkov 2003). In addition, its H I flux was measured with the 100-m radio telescope at Effelsberg (Huchtmeier, Karachentsev & Karachentseva 2000). The Arecibo ALFALFA survey showed its gas mass was quite high. Based on the literature available, KKR 17 has been poorly studied and could be an ideal laboratory to test star-formation models.

In this paper, we explored the global properties of KKR 17, using multi-wavelength observations from the ultraviolet (UV) to the near-infrared (NIR), mainly focusing on star formation and the stellar population. The observations and relevant data reduction are presented in Section 2. The main results of our analysis are presented in Section 3. The discussions and summary are presented in Sections 4 and 5, respectively.

2 OBSERVATION AND DATA REDUCTION

We used archived far-UV (FUV) and near-UV (NUV) images from *Galaxy Evolution Explorer* (*GALEX*), optical wide-band images (*ugriz*) from Sloan Digital Sky Survey (SDSS), mid-infrared 3.4-µm images from *Wide-Field Infrared Survey Explorer* (*WISE*) and H I data from ALFALFA. In addition, we obtained optical narrow-band images and spectra of KKR 17 using the BAO Faint Object Spectrograph and Camera (BFOSC) mounted on the 2.16-m telescope at Xinglong Observatory, National Astronomical Observatories of the Chinese Academy of Science (NAOC). Detailed information is given in Table 1.

2.1 Ultraviolet images

The *GALEX* mission was launched in 2003, and it surveyed the whole sky simultaneously in two broad bands. The effective wavelength of the FUV instrument was 1516 Å and that of the NUV instrument was 2267 Å (Martin et al. 2005). The field of view (FOV) of *GALEX* was $\sim1.2^{\circ}$ (Morrissey et al. 2007). We obtained images from the *GALEX* Medium Imaging Survey (∼1500 s), which was designed to cover 1000 deg^2 and reach to $m_{AB} \approx 23$ mag. This survey covered the maximum area of the SDSS survey. The keywords of mean sky-background level (SKY) and AB magnitude zero-point (ZP) in the header of image were used for sky subtraction and flux calibration, respectively. The final image has a spatial resolution of 6 arcsec and a pixel size of 1.5 arcsec.

2.2 Optical images

The optical broad-band images (*ugriz*) were taken from the SDSS data archive server (York et al. 2000; Stoughton et al. 2000). The background was subtracted from each image before photometry, and the counts were converted into flux densities and magnitudes.

New images with narrow-band filters (centred at red-shifted H α and [O III]) and broad-band filters (*V*- and *R*-bands) were observed with BFOSC on the 2.16-m telescope at Xinglong Observatory, NAOC, on 2012 June 16. The FOV of BFOSC is approximately 8.5 arcmin × 9.5 arcmin and the CCD size is 1130 × 1230 pixels. One pixel of BFOSC corresponds to ∼0.45 arcsec. The continuum-subtracted [O III] images included both [O III] $\lambda\lambda$ 4959 and 5007 in our images. However, the continuum-subtracted Hα images still included a component from [N II] $\lambda\lambda$6548, 6583 emission lines. Fortunately, the doublet [N II] lines were very weak in the low-metallicity environment, which could contaminate at most ∼5 per cent of the fluxes in our narrow-band images and are much less than the flux calibration error. Therefore, we neglected the [N II] emission lines from KKR 17 in our analysis.

All standard CCD reductions were performed before astrometric and flux calibrations. The SDSS field stars were used as references for astrometric and flux calibration, and the astrometric calibration accuracy was better than 1 arcsec in our images. Flux calibrations were converted between SDSS and UBVR$_c$I$_c$ magnitude systems,

Downloaded from http://mnras.oxfordjournals.org/ at National Astronomical Observatory on March 8, 2015

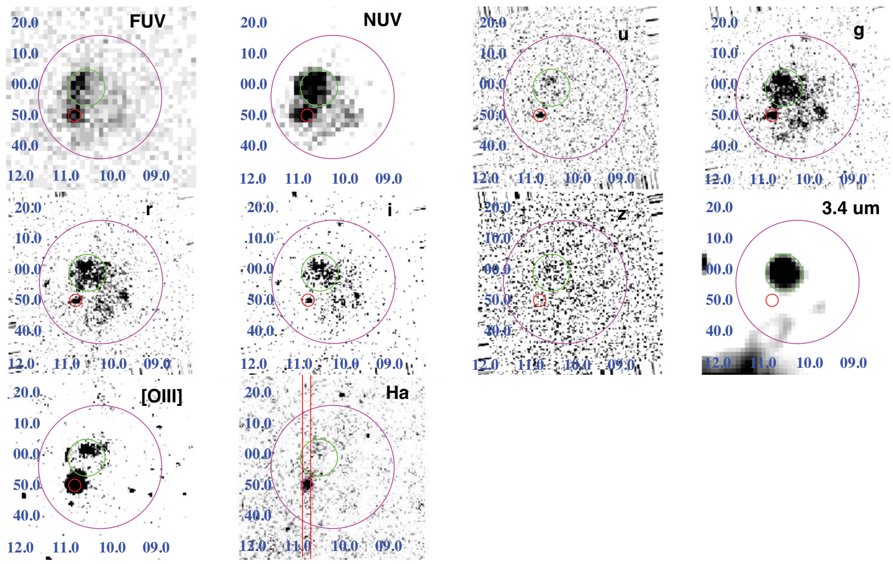

Figure 1. Multi-wavelength images of KKR 17 (centred on RA $15^{\rm h}11^{\rm m}10\overset{\rm s}{.}2$ and Dec. $+11^\circ01'56''$). From left to right and from top to bottom are FUV and NUV images from *GALEX*, *ugriz* images from SDSS, 3.4 μm image from *WISE* and [O III] and Hα narrow-band images from the 2.16-m telescope at Xinglong Observatory. The narrow-band images already had the stellar continuum subtracted. The magenta circles are our aperture circle. The spectra were extracted from region 1 (red circles). Low-mass stars are dominant in region 2 (green circles). The red lines on the Hα image indicate the position of the long slit of our spectrum.

using the conversion coefficients in Lupton (2005).[1] The *V*- and *R*-band images were used for the stellar continuum, which was subtracted from the narrow-band [O III] and Hα images. We estimated that the error of the integrated flux was less than 20 per cent in the narrow-band images, which was limited by the low surface brightness of the galaxy and the flux calibration error.

2.3 Infrared data

The infrared images of KKR 17 were taken from the *WISE* satellite (Wright et al. 2010). The mission was launched in 2009 and began to survey the whole sky in 2010. The astrometric accuracy for the high signal-to-noise (S/N) images was better than 1.5 arcsec. The angular resolution was 6.1, 6.4, 6.5 and 12.0 arcsec at wavelengths of 3.4, 4.6, 12 and 22 μm, respectively. KKR 17 (J2000) was only found at 3.4 μm due to the contamination of nearby bright stars. Moreover, as shown in Fig. 1, 3.4 μm is also contaminated by a nearby bright star. Therefore, we need to mask the bright star for the aperture photometry in this band.

2.4 H I data

ALFALFA (Giovanelli et al. 2005) is the largest blind H I line survey. The current catalogue, α.40, which covered ~40 per cent of the final targeted sky area (Haynes et al. 2011), contains ~15 000 extragalactic sources in regions for (1) spring ($07^{\rm h}30^{\rm m} < {\rm RA} < 16^{\rm h}30^{\rm m}$, $+04^\circ < {\rm DEC} < +16^\circ$ and $+24^\circ < {\rm DEC} < +28^\circ$) and (2) fall ($22^{\rm h} < {\rm RA} < 03^{\rm h}$, $+14^\circ < {\rm DEC} < +16^\circ$ and $+24^\circ < {\rm DEC} < +32^\circ$). The catalogue includes source information for position, H I fluxes, H I masses, systemic velocities, H I linewidths, etc.

The 21-cm line profile of KKR 17 is from the archived ALFALFA survey (Giovanelli et al. 2005). The H I line of KKR 17 is shown as a single-horn profile on the velocity map, which may indicate that it is a face-on or unstable-disk galaxy. The H I mass of KKR 17 is $\sim 4.37 \times 10^9$ M$_\odot$ and its distance is 120.8 Mpc (Haynes et al. 2011), which shows the mass of neutral hydrogen is comparable to that in a normal galaxy. The galaxy is receding at a velocity of 8283 ± 4 km s^{-1}, which is consistent with the Hubble flow velocity inferred from the red shift ($z = 0.0277$) of our spectral analysis.

2.5 Photometry

Photometry of data in all bands was performed after CCD pre-procedures, which included overscan subtraction, bias subtraction, flat-field correction, cosmic ray reduction and background subtraction. The IRAF task SURFIT was used for background subtraction. We used the IRAF task PHOT to produce the photometry with the same aperture, and fixed the aperture centre at RA $15^{\rm h}11^{\rm m}10\overset{\rm s}{.}2$, Dec. $+11^\circ01'56''$. The aperture radius was 20 arcsec for the entire analysis. In addition, we selected two different regions to analyse their properties: (1) the diffuse region centred on RA $15^{\rm h}11^{\rm m}10\overset{\rm s}{.}5$, Dec. $+11^\circ01'59''$ with photometric aperture radius of 6 arcsec and (2) the H II region centred on RA $15^{\rm h}11^{\rm m}10\overset{\rm s}{.}76$, Dec. $+11^\circ01'50farcs05$, with photometric aperture radius of 2 arcsec. All the photometric results are shown in Table 2.

2.6 Optical spectra

The optical spectra of the H II region in KKR 17 were observed on 2013 March 10 (G6+1.8 arcsec), 2012 June 15 (G7+1.8 arcsec) and 2012 June 17 (G8+1.8 arcsec). The observations were also performed by BFOSC on the 2.16-m telescope. A slit with a width of 1.8 arcsec, combined with three different grisms (G6 from 3600 to 5450 Å, G7 from 4000 to 6700 Å, and G8 from 5800 to 8000 Å), were used for the observations. However, only the G6 and G8 spectra were analysed. The resolution of the grisms is ~10 Å. KKR 17 and its H II regions cannot be seen by the guide cameras of the 2.16-m telescope because their flux is quite low. So it is difficult to position the slit properly. We noticed that there was one bright star nearby in

[1] http://www.sdss.org/dr7/algorithms/sdssUBVRITransform.html

Downloaded from http://mnras.oxfordjournals.org/ at National Astronomical Observatory on March 8, 2015

Table 2. Properties of KKR 17.

Parameter	Diffuse region	H II region	Total
Optical RA (J2000)	$15^{\mathrm{h}}11^{\mathrm{m}}10\overset{\mathrm{s}}{.}5$	$15^{\mathrm{h}}11^{\mathrm{m}}10\overset{\mathrm{s}}{.}76$	$15^{\mathrm{h}}11^{\mathrm{m}}10\overset{\mathrm{s}}{.}2$
Optical Dec (J2000)	$+11°01'59''$	$+11°01'50''05$	$+11°01'56''$
Radio RA (J2000)	–	–	$15^{\mathrm{h}}11^{\mathrm{m}}07\overset{\mathrm{s}}{.}90$
Radio Dec (J2000)	–	–	$+11°02'37''$
W50 (km s^{-1})	–	–	29 ± 2
$F_{\mathrm{H\,I}}$ (Jy km s^{-1})	–	–	1.26 ± 0.05
Distance (Mpc)	–	–	120.8 ± 8.5
$M_{\mathrm{H\,I}}/\mathrm{M}_{\odot}$ [a]	–	–	4.37×10^{9}
μ_0(B) (mag sec^{-2})	–	–	24.15 ± 0.03
FUV (mag)[b]	23.29 ± 0.19	21.44 ± 0.10	19.09 ± 0.06
NUV (mag)[b]	20.14 ± 0.08	21.64 ± 0.06	19.02 ± 0.04
u (mag)[c]	19.54 ± 0.10	20.60 ± 0.12	18.43 ± 0.15
g (mag)[c]	18.72 ± 0.02	20.22 ± 0.04	17.68 ± 0.03
r (mag)[c]	18.62 ± 0.03	20.49 ± 0.07	17.49 ± 0.04
i (mag)[c]	18.48 ± 0.04	20.93 ± 0.14	17.37 ± 0.06
z (mag)[c]	18.46 ± 0.15	20.88 ± 0.44	17.18 ± 0.22
[O III] (10^{-14} erg s^{-1} cm^{-2})	0.78 ± 0.08	1.26 ± 0.03	1.86 ± 0.20
Hα (10^{-14} erg s^{-1} cm^{-2})	0.33 ± 0.08	0.64 ± 0.03	1.51 ± 0.26
3.4 μm (mag)[b]	19.98 ± 0.21	22.76 ± 0.59	18.78 ± 0.15

[a] The mass was calculated with a distance of 120.8 Mpc.
[b] In the AB system.
[c] In the SDSS system.

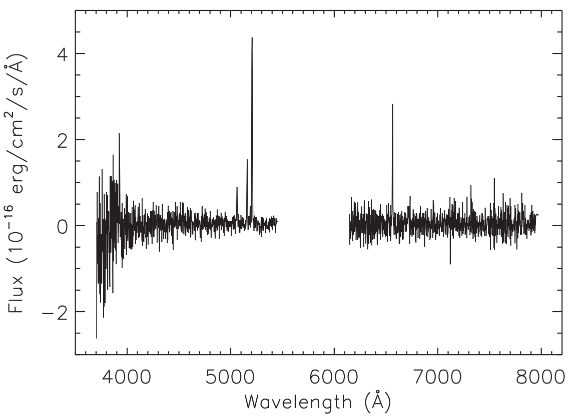

Figure 2. Spectrum of the H II region (region 1 in Fig. 1) of KKR 17.

the FOV of the guide camera, and we estimated the offset between the star and H II region through the narrow-band image. The slit was then fixed at the position with the estimated offset relative to the star. The CCD reductions including overscan and bias subtraction, flat-field correction and cosmic ray reduction, were performed before wavelength and flux calibrations. An Fe/Ar lamp was used as the wavelength standard for our spectra, and the Kitt Peak National Observatory IRS standard stars were adopted as the flux standard. The optical spectra are shown in Fig. 2 and all strong emission lines that we measured are shown in Table 3.

Table 3. Emission-line fluxes and errors.

Line	Equivalent width (Å)	Intensity (I_λ) (10^{-15} erg s^{-1} cm^{-2})
	2012 Jun 15	
	Upper aperture	
Hβ (4861 Å)	-249.5 ± 23	1.25 ± 0.10
[O III] λ4959	-667.5 ± 32	1.82 ± 0.09
[O III] λ5007	-2429 ± 645	5.13 ± 0.10
	Bottom aperture	
Hβ (4861 Å)	-552.3 ± 188	0.46 ± 0.10
[O III] λ4959	-427.9 ± 50	0.68 ± 0.08
[O III] λ5007	-3537 ± 278	1.62 ± 0.09
	2012 Jun 17	
Hα (6563 Å)*	-593.6 ± 33	1.81 ± 0.13
[N II] λ6583	-27.6 ± 36	0.10 ± 0.10
	2013 Mar 10	
[O II] λ3727	-225.9 ± 11	1.59 ± 0.11
Hβ (4861 Å)*	-212.2 ± 72	0.80 ± 0.10
[O III] λ4959	-290.1 ± 40	1.23 ± 0.10
[O III] λ5007	-610.7 ± 16	3.85 ± 0.09

* The high $I(\mathrm{H}\beta)/I(\mathrm{H}\alpha)$ ratio of KKR 17 is due to double-components of the Hβ emission line. The spectra resolution was limited by the telescope aperture, and it is a small telescope in our case. The spectral resolution of the 2.16-m telescope is only ∼10 Å, which makes it challenging to distinguish the precise sub-structures of KKR 17. Also, the observation seeings on two days were different, which may lead to a small position deviation between two spectra.

3 RESULTS

3.1 Multi-wavelength morphologies in KKR 17

KKR 17 is an irregular, gas-rich galaxy. It has a significant bright H II region and a very diffuse, faint region. Fig. 1 shows the different band images from FUV to NIR and the continuum-subtracted [O III] and Hα images. We separated KKR 17 into two different parts, and discuss their different spectral energy distributions (SEDs) and stellar populations in the following sections. KKR 17 has different morphologies seen from UV to NIR, and also centred on different regions in different bands. The H II region was the brightest in FUV and NUV; in contrast, the diffuse region was also bright in NUV,

Downloaded from http://mnras.oxfordjournals.org/ at National Astronomical Observatory on March 8, 2015

but faint in FUV. In addition, in the optical u band, which has a low sensitivity, the H II and diffuse regions have different features: the diffuse region was barely detectable, but the H II region was still bright enough for detection. The optical g-, r- and i-band images show very similar morphologies for KKR 17. This galaxy has an unstable-disk feature in the g-, r- and i-bands. However, the g- and r-band images are contaminated by [O III] and Hα emissions, respectively. The narrow-band [O III] image with the continuum subtracted shows the emission from the bright H II knot is relatively stronger than from the diffuse region, although the radiation fields in both the bright H II knot and diffuse region are strong. However, only the narrow-band Hα image shows the bright H II region, which indicates the H II knot is undergoing relatively strong star-formation activity. The low-sensitivity optical z-band image was faint for both regions. The 3.4 µm emission is dominated by late-type stars centred at RA $15^{\mathrm{h}}11^{\mathrm{m}}10\overset{\mathrm{s}}{.}5$, Dec. $+11°01'59''$, which may be the real galactic centre. The disappearance of the H II region at 3.4 µm also reveals that the mass of this region is relatively small.

3.2 Surface brightness

To obtain the surface brightness profile of KKR 17, we first adopted a geometric centre from the NASA/IPAC Extragalactic Database and decomposed the galaxy structure using GALFIT (Peng et al. 2002). Since KKR 17 is bulgeless (Sérsic index <1), we fitted the galaxy with a single-exponential profile. We obtained the semi-axis ratio $b/a = 0.92$, the inclination 34.90° and the disk scale length $r_s = 7.52$ arcsec. The galactic scale length is equivalent to the linear scale length of 4.20 kpc at this red shift, which is comparable to nearby giant LSBG Malin 1 (Barth et al. 2007). Then, we performed concentric elliptical aperture photometry based on GALFIT's results. The surface brightness profile of KKR 17 in the g-band is shown in Fig. 3. The colour $g - r \sim 0.15$ mag.

To obtain the central surface brightness, we converted the SDSS magnitude to a Johnson B-band magnitude (Lupton 2005). Then we used the following relation from Galaz et al. (2011) to calculate the surface brightness of KKR 17:

$$\mu_0(B) = B + 2.5\log(2\pi a^2) + 2.5\log(b/a) - 10\log(1 + z). \quad (1)$$

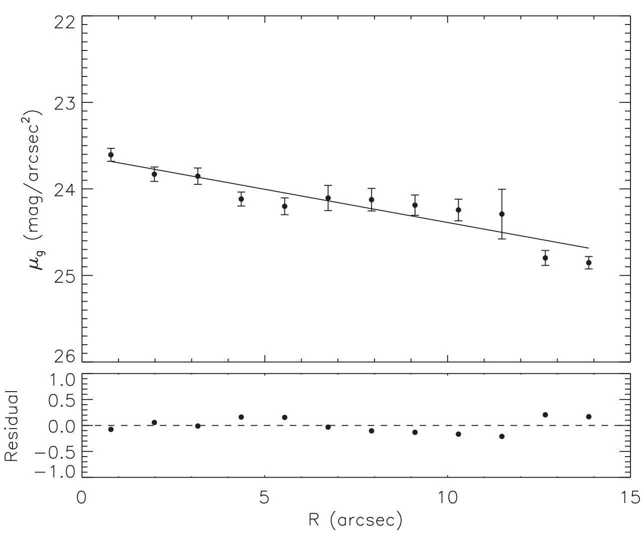

Figure 3. Surface brightness profile of KKR 17. The solid line shows the best-fitting single-exponential component. The best fit is consistent with the outer region of the galaxy and the GALFIT decomposition results.

The semi-axis ratio and red shift are from the GALFIT results. The central surface brightness of KKR 17 was found to be $\mu_0(B) = 24.14 \pm 0.03$ mag s^{-2}.

3.3 Stellar population

The colour of a galaxy can reveal its star-formation history (SFH): an older stellar population has a redder colour and a younger stellar population has a bluer colour. Previous studies have found the ages of blue LSBGs span a wide range, from young (2 Gyr) (Zackrisson, Bergvall & Östlin 2005) to old (∼7 Gyr) (Jimenez et al. 1998), which depends on both the physical conditions in the disk and SFR (Vorobyov et al. 2009). One explanation for these blue LSBGs is that they may be formed by episodic star formation (e.g. McGaugh 1994a; Gerritsen & de Blok 1999; Bothun et al. 1997). This means the stars could form through a discrete process with small perturbations. The star-formation process could have both active and quiescent periods in the galaxy and last for a few gigayears. The global stellar population has a low SFR, and the bright H II region was formed by episodic star formation. KKR 17 is classified as a very blue LSBG, based on a definition by O'Neil et al. (1997) (the $U - B$ and $B - V$ colours of KKR 17 are 0.25 and 0.27, respectively). It has a significant bright H II region and a faint diffuse region, which would be a perfect test bed for theoretical models of LSBGs.

The FUV-to-optical SED of the total area, diffuse region and H II knot of KKR 17 are shown in Fig. 4. We compared the SEDs of KKR 17 with different morphological templates to determine the stellar population. We used SED templates of elliptical and late-type spiral galaxies, and low-dust extinction starburst galaxies (with reddening $E(B - V) < 0.1$) from Kinney et al. (1996), and also took one spectrum of a typical LSBG, UGCA357 (van Zee et al. 1997). We normalized the fluxes of the templates and KKR 17 with the central wavelength of the i-band filter, which can mitigate for the strong emissions of [O III] and Hα. The total continuum for KKR 17 seems to be flatter compared to those of late-type and starburst galaxies. The hybrid stellar population is revealed, which could be a combination of the populations for spiral Sc galaxies and ellipticals. The H II knot is a typical young-star-dominated region. However, the stellar population of the diffuse region is quite different from that of the H II knot. The diffuse region has a jump in the flux between NUV and FUV, which is a typical spectral feature for A-type stars (Gulati et al. 1994). Thus, the diffuse region may be dominated by A-type stars. Hence, the diffuse region makes the largest contribution to the mass of the galaxy, which is consistent with the NIR 3.4-µm image.

To derive the visible stellar population in a more precise way, we used stellar evolutionary tracks for a single stellar population (SSP) with the Salpeter initial mass function (IMF) (Salpeter 1955). The stellar evolutionary tracks were calculated based on the SSP models of Bruzual & Charlot (2003) with an instantaneous star formation law, which is effective for episodic star formation and instantaneous starbursts. For KKR 17, the best metallicity O/H value adopted was $Z = 0.004$ (see Section 3.5). Fig. 5 shows the *ugr* colour–colour diagram of the entire galaxy, H II region and diffuse region. We considered cases with and without emission lines subtracted. The integrated $(u - g)$ and $(g - r)$ colours of the entire galaxy and diffuse region correspond to an age of ∼600 Myr. The H II region is much younger than the diffuse region: the integrated colours reveal that the age of the stellar population of this region is ∼40 Myr. However, the age of the H II region was hard to define after the emission lines were subtracted because the emission lines in the H II region are

Downloaded from http://mnras.oxfordjournals.org/ at National Astronomical Observatory on March 8, 2015

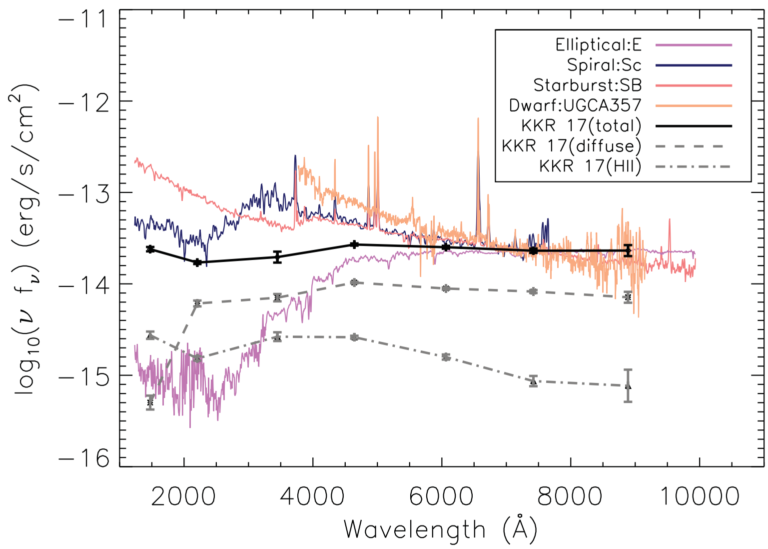

Figure 4. Spectral energy distributions of KKR 17, including the global, diffuse and bright H II regions. The templates of different types of galaxy (E-Sc) are shown from the Kinney–Calzetti Spectral Atlas of Galaxies (Kinney et al. 1996). The dwarf template is the spectrum of the typical LSBG, UGCA357 (van Zee, Haynes & Salzer 1997). This figure shows that KKR 17 contains a large fraction of old stars, comparable to an elliptical galaxy. However, the fraction of young stars is lower than in UGCA357 but comparable to a Sc-type spiral galaxy.

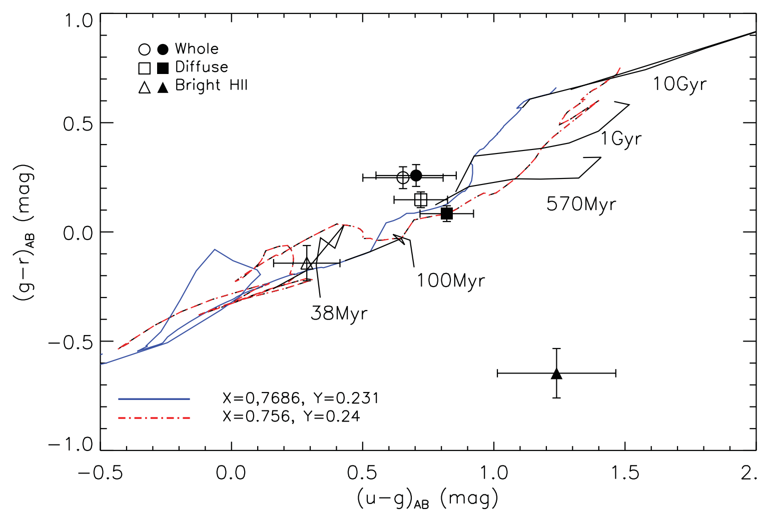

Figure 5. *ugr* colour–colour diagram of the entire galaxy KKR 17 (circles), H II region (squares) and diffuse region (triangles) with error bars. Open symbols are for regions without emission lines subtracted ([O III] and Hα). Solid symbols are for regions with emission lines subtracted (for a further description, see Section 3.3). The stellar evolutionary tracks use the SSP models of Bruzual & Charlot (2003) under the instantaneous SF law. The stellar metallicity adopted was $Z = 0.004$, which is the best model for the gas metallicity. Blue solid line: Stellar track with $X = 0.7686$ and $Y = 0.231$. Red dotted-dash line: Stellar track with $X = 0.756$ and $Y = 0.24$. Black solid lines: Isochrone lines for 38 Myr, 570 Myr and 10 Gyr.

strong. Additionally, it was hard to detect the continuum in the H II region.

The flux over the wavelength range of H II for both the SED and stellar synthesis model was similar to those of OB stars clusters, which to some extent means the H II region is undergoing star formation. However, the existence of a large fraction of medium age stars (∼600 Myr) in the diffuse region may also be seen as a hint of different star-formation histories in the two regions.

3.4 Stellar mass

The stellar mass of a galaxy is a crucial fundamental parameter for galaxy evolution. The mass-to-light ratio relation and single NIR luminosity can be used as useful estimators for the stellar masses. All the methods of constraining the stellar mass of galaxies suffer from an uncertainty of a factor of 2 (McGaugh & Schombert 2013) because of a large uncertainty in the contribution fraction of the thermally pulsing asymptotic giant branch (TP-AGB) stars in the stellar evolution model. The TP-AGB stars have been found to dominate at some evolutionary phases for galaxies (Bruzual 2007a). Many evolutionary tracks are biased when the TP-AGB contribution in stellar population synthesis models is considered. For example, the galaxy masses derived from models by Bruzual 2011 and Bruzual 2007b are much lower than that derived from Bruzual & Charlot 2003. In this paper, three different methods were adopted to check the consistency of the stellar mass of KKR 17.

Downloaded from http://mnras.oxfordjournals.org/ at National Astronomical Observatory on March 8, 2015

(1) Optical mass-to-light ratio: The mass-to-light ratio (M/L) is an effective way to estimate stellar masses with small changes from model to model. The mass-to-light ratio properly falls within the reasonable range of IMF. Cole et al. (2001) and Bell et al. (2003) derived M/L and studied the stellar mass function by combining the NIR and optical photometry for a sample dominated by normal galaxies. de Blok, McGaugh & Rubin (2001) suggested the B-band stellar mass-to-light ratio (M/L_{B}) was around 1.4 for LSBGs. Under this assumption, the stellar mass for KKR 17 was estimated based on the B-band absolute magnitude in Freeman (1970), as $1.32 \times 10^9\,\mathrm{M}_{\odot}$.

(2) Optical colours: We also adopted the optical $(g - r)$ colour from Bell et al. (2003) to check the stellar mass derived from M/L_{B}. We used the following conversion:

$$\log \frac{M_{\star}}{\mathrm{M}_{\odot}} = 0.4(M_{r,\mathrm{AB}} - 4.67) + [a_r + b_r(g - r)_{\mathrm{AB}} + 0.15] \quad (2)$$

where $M_{r,\mathrm{AB}}$ is the r-band absolute magnitude and $(g - r)_{\mathrm{AB}}$ is the rest-frame colour in the AB magnitude system. The coefficients a_r and b_r were adopted as -0.306 and 1.097, respectively. The derived stellar mass of KKR 17 with the relation above is $1.22 \times 10^9\,\mathrm{M}_{\odot}$, which is close to that of the previous method. As we can see, both results show that the stellar mass of the galaxy is more than two times lower than the mass of neutral hydrogen, which indicates that KKR 17 is dominated by neutral hydrogen. The gas fraction of KKR 17 is $f_{\mathrm{gas}} \equiv \log(M_{\mathrm{gas}}/(M\star + M_{\mathrm{gas}})) = -0.08$. Its gas ratio $\log(M_{\mathrm{gas}}/M\star) = 0.71$, which is a factor of 2 below the average gas fraction ($\log(M_{\mathrm{gas}}/M\star) \sim 1.5$) for 40 per cent of the Arecibo ALFALFA total sample (Huang et al. 2012).

(3) Monochromatic 3.4 μm luminosity: This is a convenient way to estimate the stellar mass since it has a lower dependence on SFH and massive stars. Previous studies have found the 3.4 μm luminosity could be a stellar mass tracer of galaxies (Wen et al. 2013), and we used the following conversion:

$$\log \frac{M_{\star}}{\mathrm{M}_{\odot}} = (-0.040 \pm 0.001) + (1.120 \pm 0.01) \times \log\left(\frac{\nu L_{\nu}(3.4\,\mu\mathrm{m})}{\mathrm{L}_{\odot}}\right). \quad (3)$$

This gives the stellar mass of KKR 17 as $3.77 \times 10^8\,\mathrm{M}_{\odot}$, which is only one-third of the stellar mass derived from M_{B}/L.

The stellar masses derived from the optical and NIR luminosities are quite different. A possible explanation is that the stellar mass estimate depends on the TP-AGB model. The NIR luminosity in method 3 may underestimate the stellar mass. In addition, method 2 is less affected by assumptions compared to method 1, and our adopted stellar mass of KKR 17 in this paper is $1.22 \times 10^9\,\mathrm{M}_{\odot}$.

3.5 Oxygen abundance

Generally, LSBGs are metal poor ($Z < 1/3\,\mathrm{Z}_{\odot}$) (McGaugh 1994b). Some of them are the most metal-poor extragalactic objects discovered so far. The signal-to-noise ratio (S/N) of [O III] λ4363 for KKR 17 was not high enough, so we only calculated the oxygen abundance for the bright H II region using the strong-line method described in McGaugh (1991) as following:

R_{23}:([O III] λλ4959, 5007 + [O II] λ3727)/Hβ,

O_{23}:([O III] λλ4959, 5007/[O II] λ3727).

Using the R_{23} and O_{23} values, the H II region of KKR 17 is superimposed on a grid of theoretical models and the abundance is determined by interpolating between the model points (see Fig. 6). The models used for this work are from McGaugh (1991) in which the massive star produced from the IMF has an upper limit of 60 $\mathrm{M}_{\odot}$.

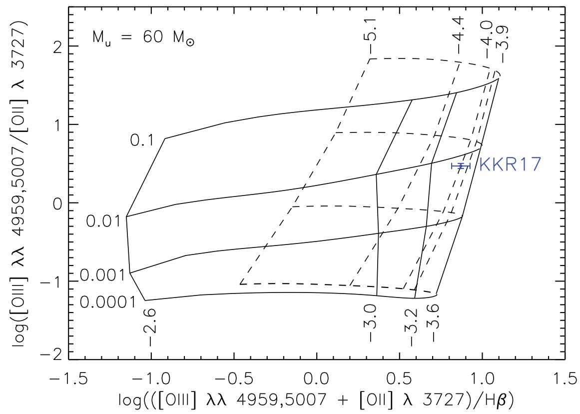

Figure 6. Diagnostic diagram of oxygen emission-line ratios compared with the photoionization models of McGaugh (1991). The position of KKR 17 indicates an oxygen abundance of $12 + \log(\mathrm{O/H}) = 8.0 \pm 0.1$.

The well-studied behaviour of the strong oxygen lines (i.e. the R_{23} parameter) with different metallicity has been scaled to the oxygen abundance, using both empirical and theoretical methods (e.g. Edmunds & Pagel 1984; McGaugh 1991; Kewley & Dopita 2002; Nagao, Maiolino & Marconi 2006), which is the foundation of all these models. The ionization parameter can also be determined based on the additional parameter O_{23}, which leads to a more accurate estimate of the abundance (e.g. Kewley & Dopita 2002; Nagao et al. 2006). However, the relationship between O_{23} and R_{23} is not unique. There exist two branches of models: (1) where oxygen abundance decreases with an increase in R_{23} for the high-metallicity branch and (2) where oxygen abundance increases with an increase in R_{23} for the low-metallicity branch. In brief, each point on the grid of McGaugh's models can lead to two different possible metallicity values.

To break the degeneracy, the [N II]/[O II] ratio is used as a diagnostic to determine whether the H II region belongs to the high- or low-metallicity branch. For KKR 17, the H II region is located on the low-metallicity branch since [N II]/[O II] <-1 and the metallicity is $12 + \log(\mathrm{O/H}) = 8.0 \pm 0.1$.

3.6 Star-formation rates

SFR is an important parameter for star-formation activities as well as the evolutionary history of galaxies. SFR tracers have been explored in a wide wavelength range from UV to sub-millimetre (e.g. Kennicutt 1998; Wu et al. 2005; Zhu et al. 2008; Calzetti et al. 2010), especially in the IR band since it is closely related to H II regions. KKR 17 is a typical LSBG. However, since the IR emissions are contaminated by nearby bright stars, we adopted the narrow-band Hα as the star-formation tracer in this paper.

The total Hα luminosity of KKR 17 was determined from the narrow-band image with both the background and continuum subtracted, by integrating the flux over the aperture that encloses the entire galaxy. The total Hα flux we obtained for KKR 17 was $(1.51 \pm 0.26) \times 10^{-14}$ erg s^{-1} cm^{-2}, or $L(\mathrm{H}\alpha) = (2.65 \pm 0.46) \times 10^{40}$ erg s^{-1} for a distance of

Downloaded from http://mnras.oxfordjournals.org/ at National Astronomical Observatory on March 8, 2015

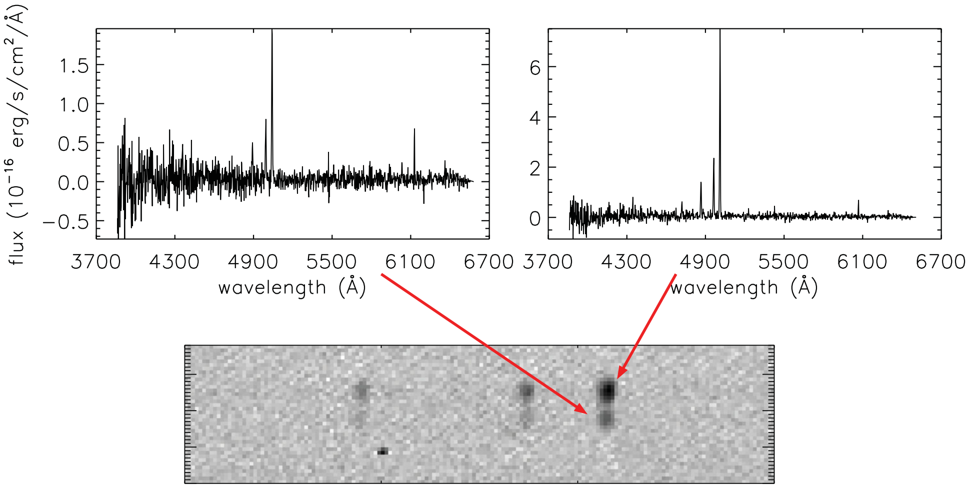

Figure 7. Sub-structure spectra of the H II region. Left: Bottom aperture. Right: Upper aperture. Hβ and [O III] $\lambda\lambda$4959,5007 have slightly different velocities in two regions. Also, the ratios of [O III] $\lambda\lambda$4959,5007 in the two regions are slightly different. The flux units are erg s^{-1} cm^{-1} Å^{-1} for the spectra.

120.8 ± 8.5 Mpc. To estimate the global SFR, we adopted the following relation (Kennicutt 1998):

$$\text{SFR}\ (\text{M}_\odot\ \text{yr}^{-1}) = 7.9 \times 10^{-42}\ L(\text{H}\alpha)(\text{ergs s}^{-1}). \quad (4)$$

This yields the total SFR $=0.21 \pm 0.04$ M$_\odot$ yr^{-1}, and the specific SFR (sSFR) is 1.80×10^{-10} yr^{-1}, using the result of Bell et al. (2003), which means the timescale to form the total mass of KKR 17 for this SFR is 10^{10} yr. The sSFR is slightly higher than for typical E/S0 galaxies inferred for an IR-selected sample (Lam et al. 2013). Therefore, we conclude that star formation in KKR 17 is still episodic.

The flux from the H II region is roughly 43 per cent of the total Hα flux of the narrow-band image, which is consistent with the results of Schombert et al. (2013). The SFR in the H II region is 0.09 ± 0.02 M$_\odot$ yr^{-1}, which is similar to the SFRs of young stellar clusters in M51 (Calzetti et al. 2005), a major merging system Arp 24 (Cao & Wu 2007), and a minor merger galaxy NGC 7479 (Zhou et al. 2011).

4 DISCUSSION

4.1 Bright H II region

KKR 17 has a clearly bright H II region on its east side, dominated by massive O stars. The H II region of KKR 17 is more compact and luminous than for the sample of Schombert et al. (2013). The total Hα luminosity of this H II region is approximately $\log L(\text{H II}) = 40.06$ erg s^{-1} within a radius of ∼1 kpc. If the luminosity of a single O7V star in a H II region is $\log L(\text{H II}) = 37.0$ (Werk et al. 2008; Schombert et al. 2013), then thousands of O stars may exist in the H II region, and they would contribute ∼50 per cent to the Hα luminosity of KKR 17, which is consistent with the previous results of van Zee (2000) and Schombert et al. (2013).

The emission lines for the H II region in KKR 17 show that star formation may be complicated. Fig. 7 shows two components in the same region of KKR 17. The physical separation of the two components is ∼1.8 kpc, which is similar to the size of the H II region. The components had a small velocity difference of ∼60 km s^{-1} identified by the [O III] emission lines, and ∼90 km s^{-1} by Hβ emission line. Also, the metallicities were slightly different in terms of the R_3 index, which can be easily obtained as a rough metallicity estimator but has a relatively large uncertainty. It can be obtained through the simple relation $R_3 = 1.35 \times I_{[\text{O III}]5007}$ (Vacca & Conti 1992), where $I_{[\text{O III}]5007}$ is the flux of [O III]. Once the value of R_3 is known, the metallicity of 12 + log (O/H) can be derived with equation (7) in Vacca & Conti (1992). For the two flux values of [O III], which correspond to different components of the H II region, the metallicity is ∼8.2 and ∼8.3, respectively, and the difference is 0.1 dex. In contrast, note that the systematic uncertainty is larger, 0.5 dex.

The small differences in the velocity and metallicity of H II components can be attributed to the internal episodic star-formation activities. In fact, young stellar clusters (YSCs), often found in HSBGs, can generate shocks, which can be used to explain those differences (Elmegreen 2004). Schombert et al. (2013) pointed out that star-formation processes in LSBGs are the same as those in HSBGs. In addition, research on YSCs in HSBGs found that YSCs are more readily formed in a cluster complex than in an isolated environment (Bastian et al. 2005). The strong stellar wind from clustering massive stars could lead to these differences in YSCs. A shock-accelerated superwind has been detected for nearby galaxies M82 and NGC 839 (Rich et al. 2010). However, this was not supported by our spectra: we did not detect any line as a strong shock tracer, i.e. the [S II] lines were weak and the [N II] lines were an upper limit detection.

Another explanation is that each component has different origins. It is possible that the bright H II region is a dwarf galaxy that fell into KKR 17 from a minor merger. The blue colour of the H II region, $g - i = -0.2$, is similar to that for an irregular galaxy (Fukugita 1995), and its absolute magnitude ($M_B \sim -15$) is at the faint end of the luminosity function for local extremely low-luminosity galaxies. Moreover, the unusual colours of $B - V = 0.27$ and $U - B = 0.21$ might also imply the existence of an infalling dwarf galaxy in KKR 17. A firm conclusion requires a higher spatial resolution study for YSCs in KKR 17, e.g. such as integral field spectroscopy.

4.2 Possible evolution scenarios for KKR 17

LSBGs are usually thought to be evolving slowly across the Hubble time compared with their high-surface-brightness counterparts. The slow evolution may be connected with the low gas surface density

Downloaded from http://mnras.oxfordjournals.org/ at National Astronomical Observatory on March 8, 2015

(van der Hulst et al. 1993). If a LSBG has a lack of neighbours over small and intermediate space scales, the absence of a gravitational interaction will keep the gas in a stable situation (Bothun et al. 1993). Also, other possibilities for the slow evolution of LSBGs could be due to the large dark matter halo, or low metallicity and dust content, or different IMF (Mihos, McGaugh & de Blok 1997; O'Neil et al. 1997).

A blue gas-rich irregular galaxy, KKR 17, is located in the Local Void in the Hercules–Aquila direction. Theoretically, it may be far away from interaction in a long timescale, which would lead to a low SFR. Previous studies on the SFH of IZw 18 showed that continuous star formation at a low rate for a long time can build up the stellar mass of a galaxy (Aloisi, Tosi & Greggio 1999; Legrand et al. 2000; Annibali et al. 2013). Although the slow star-formation process cannot be confirmed, we found that KKR 17 experienced a short period of star formation roughly 600 Myr ago. Kim (2007) pointed out the LSBGs have been evolving fast in the recent ∼1 Gyr. Their results are in favour of episodic star formation (McGaugh 1992). The medium-age stellar population of the diffuse region in KKR 17 may be dominated by A-type stars, which is consistent with the result of Kim (2007).

In KKR 17, the bright H II region is currently undergoing strong star formation. The strong emission line features of the H II region indicate the existence of a large fraction of O stars. The luminosity of the H II region ($L(\mathrm{H}\alpha) > 10^{40}$ erg s^{-1}) is unusually high for a LSBG (Helmboldt et al. 2009; Schombert et al. 2013). As suggested by Bastian et al. (2006), star formation in such a complicated YSC could be triggered by an external perturbation. If the perturbation was from a nearby galaxy, we should find evidence in the observations. However, we have not found any objects from our FUV to NIR images. It is an isolated galaxy without any obvious large galaxies within an angular radius of 8 arcmin, which is equivalent to ∼250 kpc at its red shift. Based on the discussion above, the multiple components of the Hβ and [O III] emission lines may be a clue for a minor merger remnant, or that the H II region is a dwarf galaxy, as discussed in Section 4.1, and experienced a minor merger. Deep interferometric imaging of KKR 17 with high spatial resolution and velocity dispersion may clear up the confusion and reveal its real star-formation activity.

5 SUMMARY

In this paper, we present results for the metallicity and SFH of the LSBG, KKR 17, with ground-based optical images and spectra combined with space telescope archival data, and they are summarized as the following:

(1) KKR 17 is a H I-dominated LSBG with $M(\mathrm{H\,I}) = 4.37 \times 10^9$ M$_\odot$. The stellar mass is only about several 10^8 to 10^9 M$_\odot$ and the central surface brightness is $\mu_0(B) = 24.14 \pm 0.03$ mag sec^{-2}.

(2) The metallicity of the entire KKR 17 is $12 + \log(\mathrm{O/H}) = 8.0 \pm 0.1$ from the model of McGaugh (1991). However, the multiple components have a slightly different metallicities.

(3) The global SFR of KKR 17 is 0.21 ± 0.04 M$_\odot$ yr^{-1}, which is ∼1/5 of our Milky Way's. The sSFR is 1.80×10^{-10} yr^{-1}, which gives 10^{10} yr to form the total stellar mass of KKR 17. This sSFR is similar to that for E/S0 galaxies. Therefore, KKR 17 is in a quiescent star-formation stage.

(4) The fits to the optical SED and colour–colour diagrams of the diffuse and H II regions revealed different stellar populations, which may represent distinct histories of star-formation activities.

ACKNOWLEDGEMENTS

We would like to thank the staff of the 2.16-m telescope at Xinglong Observatory for their excellent support during our observing runs. We would also like to thank Dr L. J. Gou for his kind help throughout the paper. We would like to acknowledge the anonymous referee for helpful suggestions and comments.

This project is supported by the National Natural Science Foundation of China (grant 11173030), the China Ministry of Science and Technology under the State Key Development Programme for Basic Research (2012CB821800 and 2014CB845705), the National Natural Science Foundation of China (grants 11225316, 11078017, 11303038, 10833006, 10978014, 10773014 and 11403061) and the Key Laboratory of Optical Astronomy, the National Astronomical Observatories, Chinese Academy of Sciences. It is supported by the Strategic Priority Research Programme 'The Emergence of Cosmological Structures' of the Chinese Academy of Sciences', grant XDB09000000.

We thank the work of the entire ALFALFA collaboration team in observing, flagging and extracting the catalogue of galaxies used in this work. We acknowledge NASA's support in the construction, operation and science analysis of the *GALEX* mission.

Funding for the creation and distribution of the SDSS archive has been provided by the Alfred P. Sloan Foundation, the participating institutions, NASA, the National Science Foundation, the US Department of Energy, the Japanese Monbukagakusho and the Max Plank Society. The SDSS website is http://www.sdss.org. SDSS is managed by the Astrophysical Research Consortium for the participating institutions.

This publication makes use of data from *WISE*, which is a joint project of the University of California, Los Angeles, and the Jet Propulsion Laboratory/California Institute of Technology, funded by NASA.

REFERENCES

Aloisi A., Tosi M., Greggio L., 1999, ApJ, 118, 302
Annibali F. et al., 2013, ApJ, 146, 144
Barth A. J., 2007, AJ, 133, 1085
Bastian N., Gieles M., Efremov Yu. N., Lamers H. J. G. L. M., 2005, A&A, 443, 79
Bastian N., Emsellem E., Kissler-Patig M., Maraston C., 2006, A&A, 445, 471
Bell E. F., McIntosh D. H., Katz N., Weinberg M. D., 2003, ApJS, 149, 289
Bergmann M. P., Jørgensen I., Hill G. J., 2003, AJ, 125, 116
Bothun G. D., Geller M. J., Kurtz M. J., Huchra J. P., Schild R. E., 1992, ApJ, 395, 347
Bothun G. D., Schombert J. M., Impey C. D., Sprayberry D., McGaugh S. S., 1993, AJ, 106, 530
Bothun G., Impey C., McGaugh S., 1997, PASP, 109, 745
Bruzual G., Charlot S., 2003, MNRAS, 344, 1000
Bruzual G., 2007a, ASP Conf. Ser. Vol. 374, From Stars to Galaxies: Building the Pieces to Build Up the Universe, p. 303
Bruzual G., 2007b, Proc. IAU Symp. #241, Stellar Populations as Building Blocks of Galaxies, p. 125
Bruzual G., 2011, in Henney W. J., Torres-Peimbert S., eds, XIII Latin American Regional IAU Meeting, Revista Mexicana de Astronomía y Astrofísica (Serie de Conferencias). Vol. 40, p. 36
Bruzual G., Charlot S., 2003, MNRAS, 344, 1000
Caldwell N., Bothun G. D., 1987, AJ, 94, 1126
Calzetti D. et al., 2005, ApJ, 633, 871
Calzetti D. et al., 2010, ApJ, 714, 1256
Cao C., Wu H., 2007, AJ, 133, 1710
Cole S. et al., 2001, MNRAS, 326, 255
de Blok W. J. G., McGaugh S. S., Rubin V. C., 2001, AJ, 122, 2396

Downloaded from http://mnras.oxfordjournals.org/ at National Astronomical Observatory on March 8, 2015

Disney M. J., 1976, Nature, 263, 573
Edmunds M. G., Pagel B. E., 1984, MNRAS, 211, 507
Elmegreen B. G., 2004, ASP Conf. Ser. Vol. 322, The Formation and Evolution of Massive Young Star Clusters, p. 277
Freeman K. C., 1970, ApJ, 160, 811
Fukugita M., Shimasaku K., Ichikawa T., 1995, PASP, 107, 945
Galaz G., Herrera-Camus R., Garcia-Lambas D., Padilla N., 2011, ApJ, 728, 74
Gerritsen J. P. E., de Blok W. J. G., 1999, A&A, 342, 655
Giovanelli R. et al., 2005, AJ, 130, 2598
Gulati R. K., Gupta R., Gothoskar P., Khobragade S., 1994, Vistas Astron., 38, 293
Haynes M. P. et al., 2011, AJ, 142, 170
Helmboldt J. F., Walterbos R. A. M., Bothun G. D., O'Neil K., Oey M. S., 2009, MNRAS, 393, 478
Huang S. Haynes M. P., Giovanelli R., Brinchmann J., 2012, ApJ, 756, 113
Huchtmeier W. K., Karachentsev I. D., Karachentseva V. E., 2000, A&AS, 147, 187
Impey C., Bothun G., 1997, ARAA, 35, 267
Impey C. D., Sprayberry D., Irwin M. J., Bothun G. D., 1996, ApJS, 105, 209
Jimenez R., Padoan P., Matteucci F., Heavens A. F., 1998, MNRAS, 299, 123
Karachentseva V. E., Karachentsev I. D., Richter G. M., 1999, A&AS, 135, 221
Kennicutt R. C., Jr, 1998, ARA&A, 36, 189
Kewley L. J., Dopita M. A., 2002, ApJS, 142, 35
Kim J. H., 2007, PhD Thesis, Univ. Maryland, College Park
Kinney A. L., Calzetti D., Bohlin R. C., McQuade K., Storchi-Bergmann T., Schmitt H. R., 1996, ApJ, 467, 38
Lam M. I., Wu H., Zhu Y.-N., Zhou Z.-M., 2013, Res. Astron. Astrophys., 13, 179
Legrand F., Kunth D., Roy J.-R., Mas-Hesse J. M., Walsh J. R., 2000, MNRAS, 355, 891
Makarov D. I., Karachentsev I. D., Burenkov A. N., 2003, A&A, 405, 951
Martin D. C. et al., 2005, ApJ, 619, 1
McGaugh S. S., 1991, ApJ, 380, 140
McGaugh S. S., 1992, PhD Thesis, Michigan Univ., Ann Arbor
McGaugh S. S., 1994a, Nature, 367, 538
McGaugh S. S., 1994b, ApJ, 426, 135
McGaugh S. S., Schombert J. M., Bothun G. D., 1995, AJ, 109, 2019
Mihos J. C., McGaugh S. S., de Blok W. J. G., 1997, ApJ, 481, 741
Morrissey P. et al., 2007, ApJS, 173, 682
Nagao T., Maiolino R., Marconi A., 2006, A&A, 459, 85
O'Neil K., Bothun G. D., Schombert J., Cornell M. E., Impey C. D., 1997, AJ, 114, 2448
Peng C. Y., Ho L. C., Impey C. D., Rix H., 2002, AJ, 124, 266
Rich J. A., Dopita M. A., Kewley L. J., Rupke D. S. N., 2010, ApJ, 721, 505
Salpeter E. E., 1955, ApJ, 121, 161
Schombert J. M., Bothun G. D., 1988, AJ, 95, 1389
Schombert J. M., McGaugh S. S., 2014, Pub. Astron. Soc. Aust., 31, 11
Schombert J. M., Bothun G. D., Schneider S. E., McGaugh S. S., 1992, AJ, 103, 1107
Schombert J. M., McGaugh S. S., Eder J., 2001, AJ, 121, 2420
Schombert J. M., Maciel T., McGaugh S., 2011, Adv. Astron., 2011, 12
Schombert J. M., McGaugh S. S., Maciel T., 2013, AJ, 146, 41
Skillman E. D., Kennicutt R. C., Hodge P. W., 1989a, ApJ, 347, 875
Skillman E. D., Terlevich R., Melnick J., 1989b, MNRAS, 240, 563
Stoughton C. et al., 2002, AJ, 123, 485
Vacca W. D., Conti P. S., 1992, ApJ, 401, 543
van der Hulst J. M., Skillman E. D., Smith T. R., Bothun G. D., McGaugh S. S., de Blok W. J. G., 1993, AJ, 106, 548
van Zee L., 2000, ApJ, 119, 2757
van Zee L., Haynes M. P., Salzer J. J., 1997, AJ, 114, 2497
Vorobyov E. I., Shchekinov Yu., Bizyaev D., Bomans D., Dettmar R.-J., 2009, A&A, 505, 483
Wen X.-Q., Wu H., Zhu Y.-N., Lam M. I., Wu C.-J., Wicker J., Zhao Y.-H., 2013, MNRAS, 433, 2946
Werk J. K., Putman M. E., Meurer G. R., Oey M. S., Ryan-Weber E. V., Kennicutt R. C. Jr., Freeman K. C., 2008, ApJ, 678, 888
Wright E. L. et al., 2010, AJ, 140, 1868
Wu H., Cao C., Hao C.-N., Liu F.-S., Wang J.-L., Xia X.-Y., Deng Z.-G., Young C. K., 2005, ApJ, 632, 79
York D. G. et al., 2000, AJ, 120, 1579
Zackrisson E., Bergvall N., Östlin G., 2005, A&A, 435, 29
Zhou Z-M., Cao C., Meng X.-M., Wu H., 2011, AJ, 142, 38
Zhu Y.-N., Wu H., Cao C., Li H.-N., 2008, ApJ, 686, 155

This paper has been typeset from a TEX/LATEX file prepared by the author.

Downloaded from http://mnras.oxfordjournals.org/ at National Astronomical Observatory on March 8, 2015